Available online at www.sciencedirect.com

ScienceDirect

Procedia Structural Integrity 81 (2026) 514–521

Structural Integrity Procedia

www.elsevier.com/locate/procedia

VIII International Conference "In-service Damage of Materials: Diagnostics and Prediction" (DMDP 2025)

# Grounding damage of stiffened hull panels: A numerical study on orientation effects and seabed-shape-driven energy dissipation

Sulthan Raffi Hadyansyah[a,b], Brilliant Aditya Fhandy[b], Reza Kurniawan Saputra[b], Aprianur Fajri[a], Aditya Rio Prabowo[a,*], Ben Ganendra[c], Sören Ehlers[d,e], Moritz Braun[e], Quang Thang Do[f]

[a] *Department of Mechanical Engineering, Universitas Sebelas Maret (UNS), Surakarta, Indonesia*
[b] *Laboratory of Design and Computational Mechanics, Faculty of Engineering, Universitas Sebelas Maret (UNS), Surakarta, Indonesia*
[c] *Department of Civil Engineering, Ghent University, Ghent, Belgium*
[d] *Institute for Maritime Energy Systems, German Aerospace Center (DLR), Geesthacht, Germany*
[e] *Institute for Ship Structural Design and Analysis, Hamburg University of Technology (TUHH), Hamburg, Germany*
[f] *Department of Naval Architecture and Ocean Engineering, Nha Trang University, Nha Trang, Vietnam*

**Abstract**

This study integrates experimental and numerical insights from stiffened-plate penetration tests with analytical seabed geometry to interrogate grounding damage. Using a canonical indenter–plate configuration for stiffened panels, hull penetration resistance is assessed against seabed conditions represented by binormal and polynomial rock geometries. Real multibeam bathymetry is interpolated into continuous surfaces and introduced as rigid indenters, enabling direct comparison between simplified plate-level fracture mechanics and complex grounding loads. Finite element analysis (FEA) with ANSYS LS-DYNA examines three orientations: horizontal (lateral seabed intrusion), vertical (local stranding), and 45° (combined penetration/raking). Results show fracture initiation is governed by local stiffener–plate interactions. Damage evolution and absorbed energy depend strongly on seabed roughness and the projected contact area, thereby linking the fidelity of analytical rock models to penetration resistance.



*Keywords:* Grounding, Stiffened Panel, Finite Element Analysis, Seabed Geometry

## 1. Introduction

Ship grounding is among the most frequent marine casualties, accounting for roughly one-third of commercial accidents (Galić et al., 2022; Yang et al., 2023; Prabowo et al., 2023, 2024; Georgiadis et al., 2025). Two archetypes are commonly distinguished, which are powered grounding, vessel momentum governs the damage evolution, and the seabed topology dictates whether tearing initiates or sliding prevails; and stranding, the vessel settles on the seabed with negligible surge/sway, and damage accrues under tides and wave action (Simonsen and Hansen, 2000; Pedersen, 2010; Sun et al., 2017; Calle et al., 2017).

* Corresponding author. Tel.: +62-271-163-632; fax: +62-271-163-632.
*E-mail address:* aditya@ft.uns.ac.id


10.1016/j.prostr.2026.03.088

This work proposes a benchmarking study to simulate hull damage in ships subjected to grounding actions using ANSYS LS-DYNA. A ship is assumed to settle vertically on a rock. The benchmark is conducted by performing a series of indentation experiments on stiffened panels, based on the work of Alsos et al. (2009a).

## 2. Literature Review & Test Reference

In a grounding scenario, the hull is assumed to meet the seabed as a cone-like indenter. The local panel responds predominantly through membrane action, where resistance builds during indentation, plastic strains concentrate near the plate–stiffener intersections, and the stiffeners commonly fold. With sufficient force, fracture typically initiates at the base plate beside the weld along inclined through-thickness planes, as similarly explained by Amdahl and Kavlie (1992). Because a damaged hull and cargo tanks may have severe environmental consequences in events like the Exxon Valdez Oil Spill (~240,000 barrels), the study focuses on indentation mechanics, plastic deformation, and fracture resistance of stiffened panels under quasi-static stranding loads, with clear relevance to collisions.

A series of scaled indentation experiments was conducted by Wang et al. (2000) to replicate real-world grounding and collision scenarios on double-hull structures. In their study, a cone-shaped indenter was used to penetrate scaled double-hull specimens, with the nose radius varied across a wide range (300 mm, 200 mm, 100 mm, and 10 mm) to represent different seabed or bow geometries. The experimental results revealed that a larger indenter radius resulted in higher load-carrying capacity and greater energy absorption, whereas a smaller radius led to earlier hull plating rupture. These findings highlight that the geometry of the striking seabed or obstacle is crucial in determining the hull's structural resistance during grounding events.

As this kind of real experiment was considered expensive in terms of material and time, as stated in Prabowo et al. (2017) and Malsyage et al. (2025), a result of indentation tests that were conducted by Alsos et al. (2009a) can be provided as a benchmarking parameter, where in this current benchmarking study, the test geometry for grounding damage was divided into three structural components: frame, plate, and stiffener. The configurations were arranged into three primary setups: unstiffened panel (US), one flat stiffener panel (1-FB), and two flat stiffener panels (2-FB), which allowed systematic evaluation of the structural response under varying degrees of stiffening (Ridwan et al., 2023, and Fuadi et al., 2024).

### *2.1. Model Specifications*

For the benchmarking parameters used in this study, three out of five configurations were selected based on Alsos et al. (2009a), who proposed stiffening types that included both flat-bar and bulb-type stiffeners. In the present work, only the flat-bar stiffener configuration was adopted, consisting of three setups: the unstiffened panel (US), the single flat-bar stiffened panel (1-FB), and the double flat-bar stiffened panel (2-FB), as shown in Table 1.

Each panel specimen measured 1200 mm × 720 mm × 5 mm (see Figs. 1 and 2). The stiffeners were fabricated from the same material, with a thickness of 5 mm. In the 1-FB configuration, the stiffener was positioned centrally along the plate's longitudinal axis. For the 2-FB configuration (see Fig. 2), two stiffeners were symmetrically arranged, each placed 120 mm away from the plate's midline, resulting in a 240 mm spacing between them. The indenter used for all configurations was modeled as a round conical shape with a 200 mm nose radius and a 45° edge angle, representing a realistic seabed contact geometry for grounding-type indentation analysis. This geometric setup enables a direct comparison of structural response and energy absorption under varying levels of stiffening. The selected parameters also ensure consistency with previously validated experimental benchmarks, enabling a reliable numerical-to-experimental correlation. Furthermore, this configuration provides a clear basis for evaluating the influence of stiffener arrangement on the plastic onset of fracture and structural resistance.

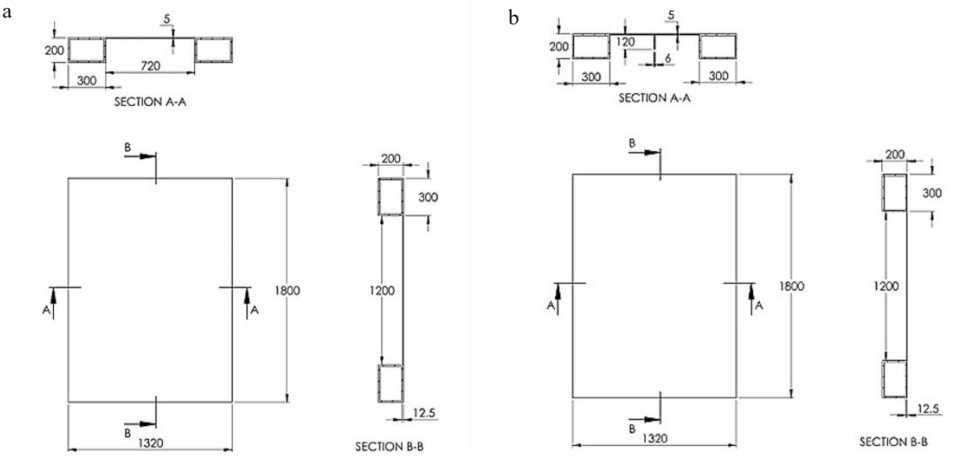


Fig. 1. Stiffened hull panel configurations: (a) Unstiffened panels (US); (b) One-flat stiffener panel (1-FB).

Table 1. Test component configurations.

| Component | Number of Stiffeners | Stiffener Type |
|---|---|---|
| US | - | - |
| 1-FB | 1 | Flat bar (FB) |
| 1-HP | 1 | Bulb (HB) |
| 2-FB | 2 | Flat bar (FB) |
| 2-HP | 2 | Bulb (HB) |

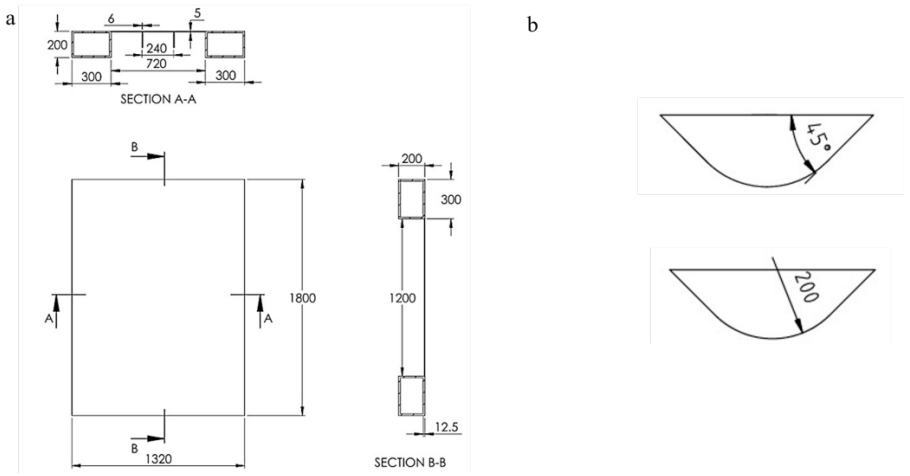


Fig. 2. Geometrical models for the finite element simulation: (a) Two-flat stiffener panel configurations; (b) Indenter configurations.

### *2.2. Materials*

The material used in this study is assumed to follow the same principle as Abubakar and Dow (2013) where the materials are considered to be isotropic and to exhibit strain hardening properties as described by Ludwik's strain hardening power law and stress-strain relation, where $\varepsilon_{plat}$ is equivalent plastic strain at the plateau strain, which was proposed by Alsos et al. (2009b) in Eqs. 1 and 2.

$$\sigma = K\varepsilon^n \tag{1}$$

and

$$\varepsilon_0 = (\frac{\sigma_y}{K})^{\frac{1}{n}} - \varepsilon_{plat} \tag{2}$$

Where $\varepsilon_0$ is computed strain offset, $K$ is the strength coefficient, $n$ is the strain hardening, and $\sigma_y$ is the yield strength.

The material used in this benchmarking study is mild steel S235JR EN10025, which is used in an unstiffened panel (US) plate, a flat stiffener panel (1-FB) plate, and two flat stiffener panels (2-FB) plates. High-strength steel S355NH-EN10210 is also used for the frame structure. In this study, all properties were taken from Alsos et al. (2009a), as described in Table 2.

Table 2. Applied material properties.

| Specimen | Materials | $\sigma_y$ [MPa] | $K$[MPa] | $n$ | $\varepsilon_{plat}$ |
|---|---|---|---|---|---|
| Plate US, 1-FB, and 2-FB | S235JR EN10025 | 285 | 740 | 0.24 | - |
| Flat Bar Stiffener | S235JR EN10025 | 340 | 760 | 0.225 | 0.015 |
| Frame | S355NH EN10210 | 390 | 830 | 0.18 | 0.01 |

### *2.3. Finite Element Model*

In this study, the material behavior of the plate and stiffener assemblies under indentation was modeled using the MAT_PLASTIC_KINEMATIC formulation in ANSYS LS-DYNA. This constitutive model was selected for its ability to

capture elastic–plastic response with strain hardening and strain-rate sensitivity, allowing realistic simulation of large plastic deformations and progressive yielding during contact with the indenter. The formulation also includes a strain-rate dependency defined by the Cowper–Symonds model, which scales the yield stress through a factor as presented in Eq. 3, which is taken from LSTC (2014).

$$1 + \left(\frac{\dot{\varepsilon}}{C}\right)^{\frac{1}{p}} \tag{3}$$

Where $\dot{\varepsilon}$ is the strain rate, a fully viscoplastic formulation is optional, incorporating the Cowper-Symonds formulation within the yield surface.

### *2.4. Meshing and Boundary Conditions*

In this benchmarking study, a range of shell element sizes, which are 5 mm, 10 mm, 15 mm, 20 mm, 25 mm, 30 mm, and 35 mm, were used. This differentiation is to model the thin-walled ship hull structure using ANSYS LS-DYNA. Shell elements were selected for their ability to capture large deformations while maintaining computational accuracy. By varying the element size, the study aimed to examine how mesh refinement influences stress distribution, structural stiffness, and overall deformation under applied loads. The boundary conditions were defined as follows: single point constraints (SPC) were applied along the bottom edges of the frame, fully constraining all translational and rotational degrees of freedom to simulate a fixed support (see Fig. 3); the indenter was modeled as a rigid body to prevent structural deformation during contact; its motion was limited to a single degree of freedom along the Y-axis to replicate the vertical indentation process. The interaction between the indenter and the panel was defined as surface-to-surface contact (LSTC, 2012), ensuring realistic load transfer and contact pressure distribution throughout the simulation.

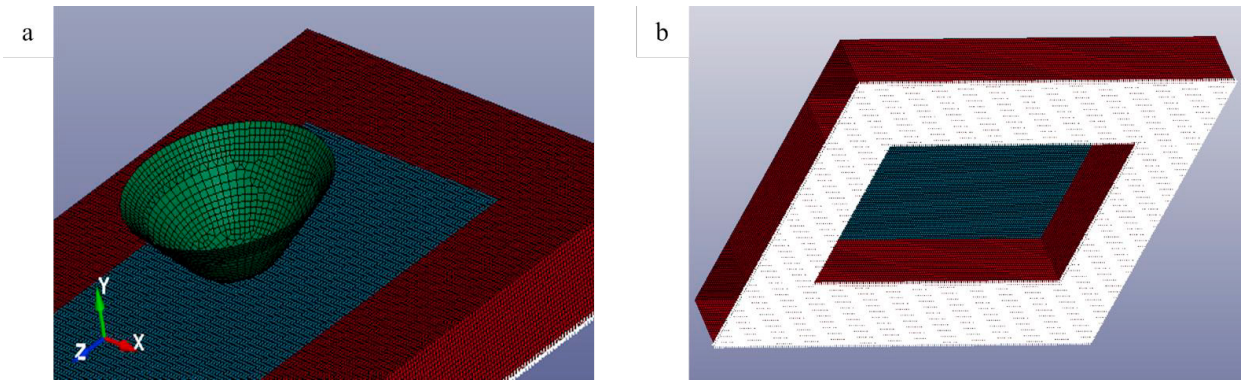


Fig. 3. Simulation setup: (a) indenter direction; (b) SPC nodes at the frame section.

## 3. Results and Discussion

The results of the benchmarking study are presented in Figs. 4–10. Based on this study, the setup configurations that demonstrated the best performance were selected and adopted as the base mesh for the future parametric study, from which all further results are derived.

### *3.1. Unstiffened panel (US)*

The FEM results obtained from ANSYS LS-DYNA illustrate the distribution of effective plastic strain after fracture. As shown in Fig. 4a, a highly localized plastic zone forms directly beneath the indenter on the left, accompanied by a crescent-shaped tear. This failure pattern closely corresponds to the experimental observations reported by Alsos et al. (2009a) and shown in Fig. 4b. In both cases, the plate exhibits pronounced out-of-plane deformation and a narrow slit oriented along the loading direction. This one-to-one correspondence between the numerical and experimental fracture morphologies provides an initial validation that the model accurately reproduces the failure mechanisms observed in the reference study.

Furthermore, the force–displacement response shown in Fig. 5 demonstrates that the simulation employing a 10 mm element mesh closely follows the reference curve from the literature. The numerical results capture both the evolution of the load gradient and the abrupt force drop occurring at a comparable displacement, indicating good agreement with the reported experimental behavior.

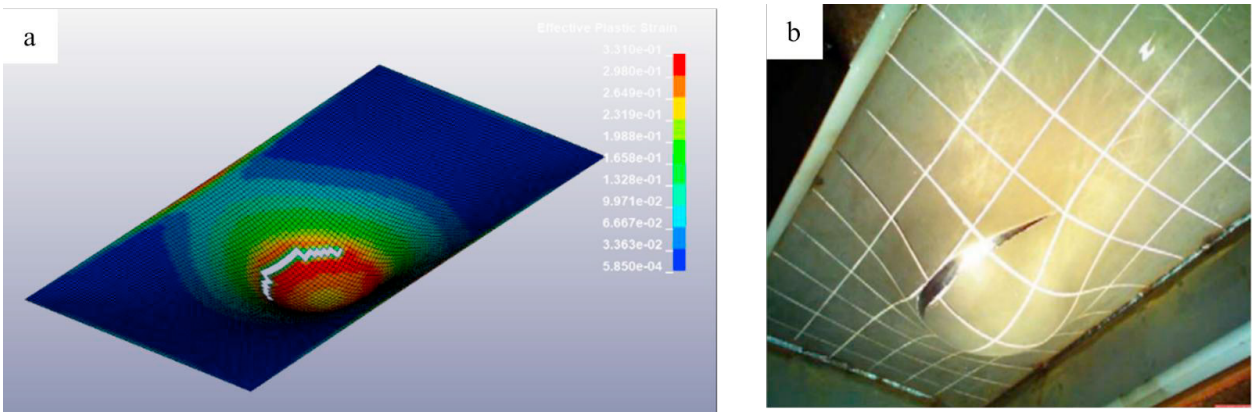


Fig. 4. Unstiffened panel (US): (a) benchmarking result; (b) experiment by Alsos et al. (2009a).

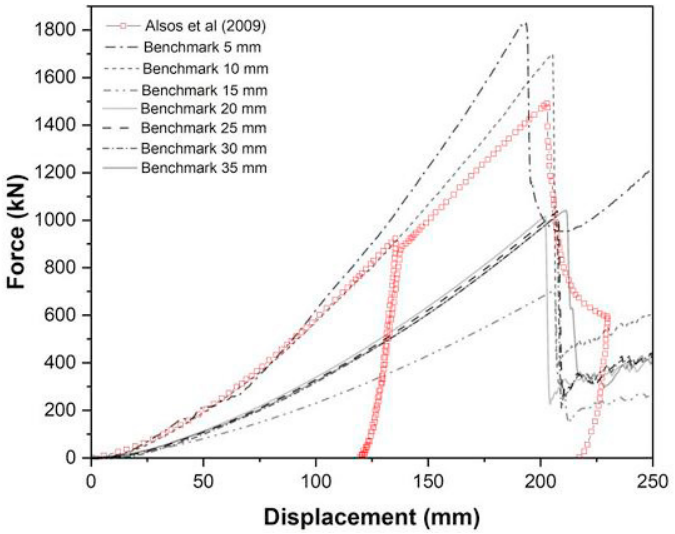


Fig. 5. Force-displacement of unstiffened panels (US).

### *3.2. One-flat stiffener panel (1-FB)*

The results in Fig. 6 show the one-stiffener panel under indentation. The ANSYS LS-DYNA results show that both pre-fracture and post-fracture conditions reveal a plastic strain pulling toward the flat bar, with tearing initiating near the stiffener. The Stiffener engagement tends to raise stiffness and peak capacity. The test photos show the same asymmetric bulge and fracture on the right side of the stiffener, validating the failure path based on the experiment by Alsos et al. (2009a) (see Fig. 7). On the force–displacement plot (see Fig. 8a), the one stiffener setup has a steeper initial slope and a lower peak force than the unstiffened one, followed by a sharp drop at 170 mm displacement. The plot also shows the 15 mm meshes, which exhibit a similar trend to the reference and a drop at a similar displacement.

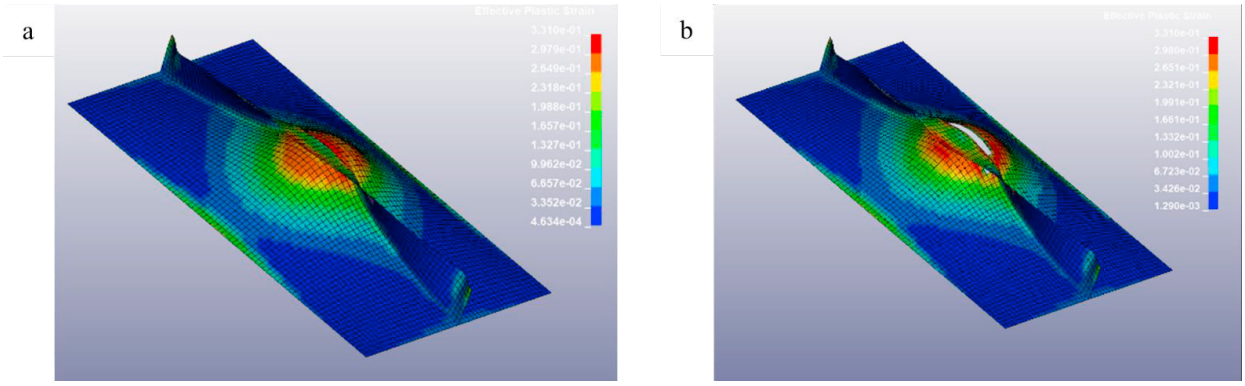


Fig. 6. Benchmarking result of 1-FB: (a) prior to fracture, and (b) after fracture.

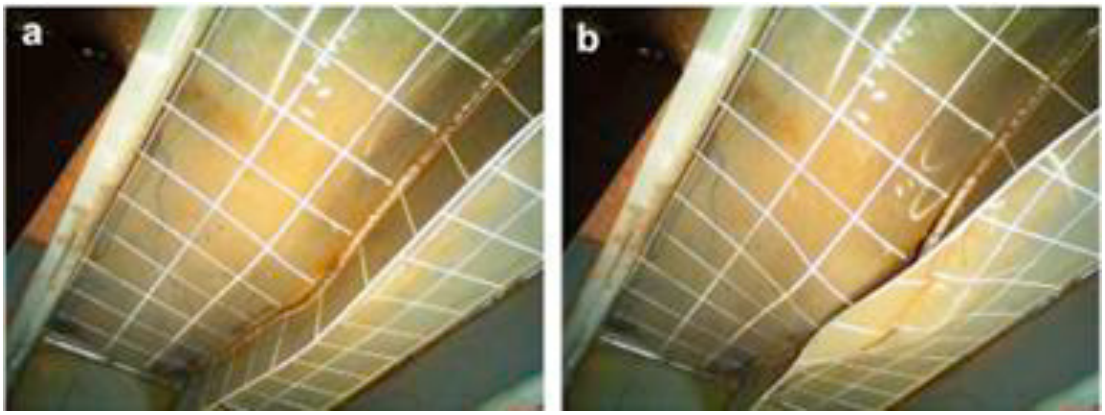


Fig. 7. Experiment results of 1-FB by Alsos et al. (2009a): (a) prior to fracture; (b) after fracture.

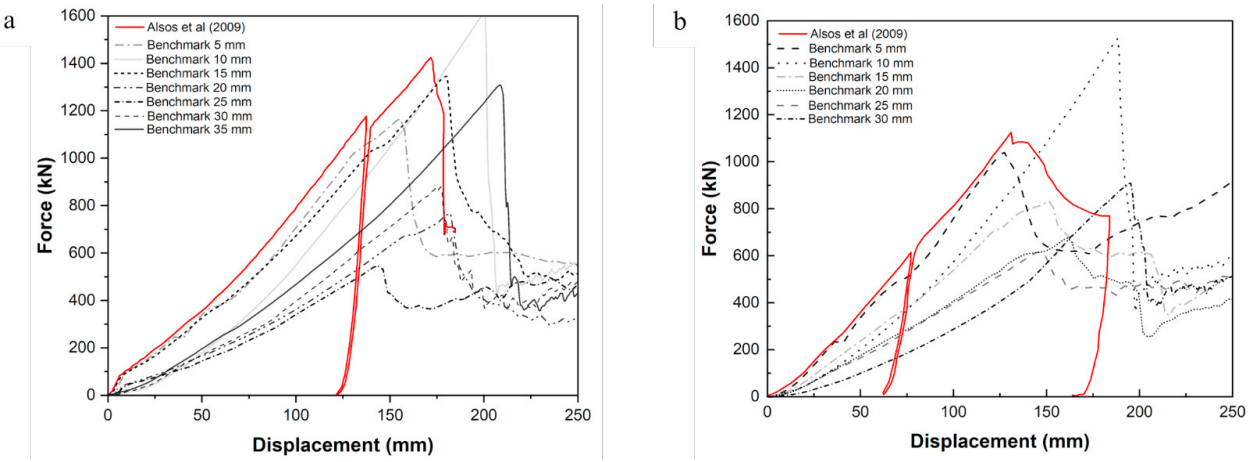


Fig. 8. Force-displacement plot: (a) one-flat stiffener panel, and (b) two-flat stiffener panel.

### *3.3. Two-flat stiffeners panel (2-FB)*

In Fig. 9, the two-stiffener panel (2-FB) behavior during simulation by ANSYS LS-DYNA, both before and after fracture, shows concentrated plastic strain between the two flat bars. From the picture in Fig. 10, the load shares a similar pattern across both stiffeners. After a while during the indentation test, tearing initiates along the stiffener line and propagates across the plate, as shown in the experimental test (see Fig. 10). The plate Section also exhibits an asymmetric bulge and a crescent-shaped tear on the right-hand side of the stiffener. On the force–displacement plot (see Fig. 8b), 2-FB shows a significant rise compared to the previous setup, then exhibits a sharp drop with a lower ultimate force compared to 1-FB and US. Furthermore, the 5 mm element mesh shows the most significant similarity to the reference trend, with a drop at a similar displacement.

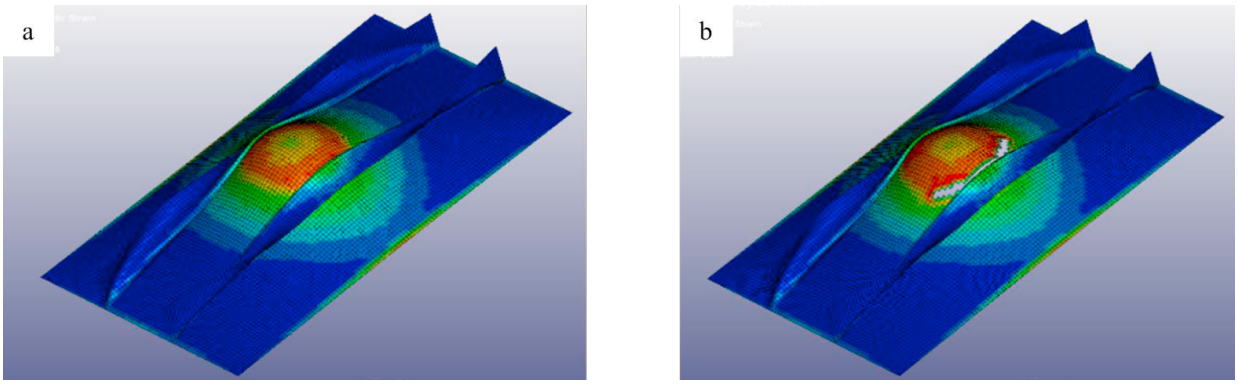


Fig. 9. Benchmarking Results of the 2-FB: (a) prior to fracture; (b) after fracture.

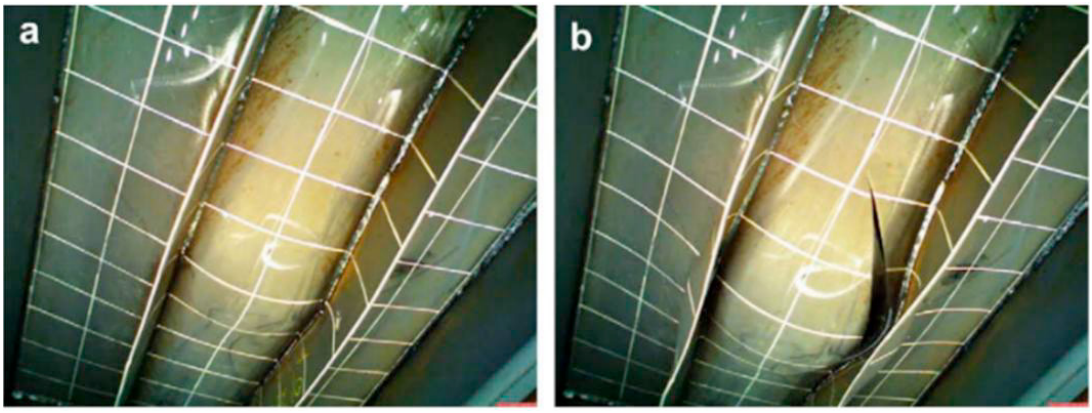


Fig. 10. Experiment Results of the 2-FB by Alsos et al. (2009a): (a) prior to fracture; (b) after fracture.

## 4. Conclusions

This benchmarking study successfully replicated the indentation behavior of stiffened hull panels, as reported by Alsos et al. (2009b), using the finite-element software ANSYS LS-DYNA. By applying the MAT_PLASTIC_KINEMATIC material model with Cowper–Symonds strain-rate dependency, the simulations accurately captured both elastic–plastic deformation and progressive fracture propagation. The mesh sensitivity analysis revealed that element sizes of 10 mm for unstiffened panels, 15 mm for single-stiffened panels, and 5 mm for double-stiffened panels provided the most consistent correlation with the experimental reference curves, accurately reflecting the load-displacement behaviour and failure modes observed in the experimental tests. The results show that stiffener configuration significantly influences overall stiffness, energy absorption, and fracture path, with increased stiffening leading to earlier fracture, lower ultimate displacement, and ultimately higher resistance. This benchmarking provides a validated foundation for further parametric studies on seabed orientation, indenter geometry, and impact energy, thereby establishing a reliable numerical framework for analyzing grounding-induced damage in ship hull structures.

## References


Abubakar, A., Dow, R. S. (2013). Simulation of ship grounding damage using the finite element method. International Journal of Solids and Structures, 50(5), 623-636.

Alsos, H. S., Amdahl, J., (2009a). On the resistance to penetration of stiffened plates. Part I: Experiments. International Journal of Impact Engineering, 36(6), 799–807.

Alsos, H. S., Amdahl, J., Hopperstad, O. S. (2009b). On the resistance to penetration of stiffened plates. Part II: Numerical analysis. International Journal of Impact Engineering, 36(6), 808–822.

Amdahl, J., Kavlie, D. (1992). Experimental and numerical simulation of double hull stranding. In DNV–MIT Workshop on Mechanics of Ship Collision and Grounding, DNV Høvik, Oslo, Norway.

Calle, M. A. G., Oshiro, R. E., Alves, M. (2017). Ship collision and grounding: Scaled experiments and numerical analysis. International Journal of Impact Engineering, 103, 195-210.

Fuadi, A. P., Muttaqie, T., Nugroho, A. C. P. T., Kurniawan, Y. F., Mukti, S., Kurniawan, M. A., Firmandha, T., Ismail, M. (2024). Patrol Boat Strengthening Against a Collision with COLL Notation Based on Class Rules and Regulation in Indonesia – An Overview. Mekanika: Majalah Ilmiah Mekanika, 23(1), 1-11.

Galić, S., Lušić, Z., Mladenović, S., Gudelj, A. (2022). A chronological overview of scientific research on ship grounding frequency estimation models. Journal of Marine Science and Engineering, 10(2), 207.

Georgiadis, D. G., Samuelides, M. S., Straub, D. (2025). Near-real-time ship grounding damage assessment using Bayesian networks. Ocean Engineering, 339, 122132.

LSTC. (2012). LS-DYNA Keyword User's Manual, Volume I – Keywords (Version 971 R6.1.0). Livermore, CA: Livermore Software Technology Corporation.

LSTC. (2014). LS-DYNA Keyword User's Manual, Volume II – Material Models (Version R7.1). Livermore, CA: Livermore Software Technology Corporation.

Malsyage, D., Bahatmaka, A., Kirana, A. C. C., Won, L. S., Hee, S. Y. (2025). Finite Element-Based Evaluation of Double-Hull Midsection Performance under Oblique Collision. Mekanika: Majalah Ilmiah Mekanika, 24(2), 121-135.

Pedersen, P. T. (2010). Review and application of ship collision and grounding analysis procedures. Marine Structures, 23(3), 241-262.

Prabowo, A. R., Bae, D. M., Sohn, J. M., Zakki, A. F., Cho, J. H. (2017). Effects of the rebounding of a striking ship on structural crashworthiness during ship-ship collision. Thin-Walled Structures, 115, 225-239.

Prabowo, A. R., Ridwan, R., Braun, M., Song, S., Ehlers, S., Firdaus, N., Adiputra, R. (2023). Comparative study of shell element formulations as NLFE parameters to forecast structural crashworthiness. Curved and Layered Structures, 10(1), 20220217.

Prabowo, A. R., Ridwan, R., Tuswan, T., Smaradhana, D. F., Cao, B., Baek, S. J. (2024). Crushing resistance on the metal-based plate under impact loading: A systematic study on the indenter radius influence in grounding accident. Applications in Engineering Science, 18, 100177.

Ridwan, R., Sudarno, S., Nubli, H., Chasan, A., Istanto, I., Pratama, P. S. (2023). Numerical Analysis of Openings in Stiffeners under Impact Loading: Investigating Structural Response and Failure Behavior. Mekanika: Majalah Ilmiah Mekanika, 22(2), 115-125.

Simonsen, B. C., Hansen, P. F. (2000). Theoretical and Statistical Analysis of Ship Grounding Accidents. Journal of Offshore Mechanics and Arctic Engineering, 122(3), 200-207.

Sun, B., Hu, Z., Wang, J. (2017). Bottom structural response prediction for ship-powered grounding over rock-type seabed obstructions. Marine Structures, 54, 127-143.

Wang, G., Arita, K., Liu, D. (2000). Behavior of a double hull in a variety of stranding or collision scenarios. Marine Structures, 13(3), 147-187.

Yang, L., Liu, J., Liu, Z., Luo, W. (2023). Grounding risk quantification in channel using the empirical ship domain. Ocean Engineering, 286, 115672.